Top Catal (2011) 54:1026–1033
DOI 10.1007/s11244-011-9722-x

ORIGINAL PAPER

Size-Selective Oxidation of Aldehydes with Zeolite Encapsulated Gold Nanoparticles

Karen T. Højholt · Anders B. Laursen · Søren Kegnæs · Claus H. Christensen

Published online: 19 August 2011

Abstract Here, we report a synthesis and catalytic study of hybrid materials comprised of 1–3 nm sinter-stable Au nanoparticles in MFI-type zeolites. An optional post-treatment in aqua regia effectively remove Au from the external surfaces. The size-selective aerobic aldehyde oxidation verifies that the active Au is accessible only through the zeolite micropores.

Keywords Catalysis · Gold · Zeolite · Aerobic oxidation · Size-selectivity

1 Introduction

Supported gold nanoparticles with a diameter of less than 10 nm are highly active oxidation catalysts for many reactions [1]. However, these catalysts frequently deactivate as the average size of the supported metal nanoparticles increases due to sintering [2–5]. Several methods have been developed to produce sinter-stable nanoparticle catalyst, including encasing the metal nanoparticles in a protective shell or in a mesoporous silica matrix [6–9]. Generally all of these materials are non-selective in their catalytic activity. One option for enhancing selectivity is encapsulating the nanoparticles in a zeolite matrix. Zeolites have an inherent micropore system of molecular dimensions, which allows for shape-selective catalysis. Furthermore, zeolites are often materials with a high thermal stability and remarkably high surface areas. These properties also make zeolites particularly useful as the catalyst in several applications, and this use of zeolites has indeed received significant attention [10, 11]. Therefore, hybrid materials consisting of nanoparticles, which are only accessible via the micropore system of zeolites are interesting as they will combine the benefits of sinter-stable nanoparticles with the shape-selective properties of zeolites. Several authors [12–15] have entrapped metal nanoparticles in the cages of zeolite crystals using post treatment methods. This type of hybrid material though, is restricted to zeolites the structure of which contains cages.

Recently, we have reported the synthesis of immobilized Au nanoparticles in silicalite-1 type crystals [16]. It was demonstrated that Au nanoparticles are primarily encapsulated in the zeolite crystals but are also present as larger agglomerates on the external surface of the zeolite. By calcination experiments both ex situ and in situ it was shown that the encapsulated Au nanoparticles are highly stable towards sintering up to a temperature of 500 °C.

Here, we present a new and improved 2-step synthesis route to encapsulate Au metal nanoparticles in ZSM-5 zeolite crystals. Besides being a 2-step synthesis, this new

K. T. Højholt · A. B. Laursen (✉)
Haldor Topsøe A/S, Nymøllevej 55, 2800 Kgs, Lyngby, Denmark
e-mail: a.b.laursen@fysik.dtu.dk

K. T. Højholt
e-mail: kntl@topsoe.dk

K. T. Højholt · S. Kegnæs
Department of Chemistry, Technical University of Denmark, Center for Catalysis and Sustainable Chemistry, 2800 Kgs, Lyngby, Denmark
e-mail: skk@kemi.dtu.dk

A. B. Laursen
Department of Chemical Engineering & Department of Physics, Center for Individual Nanoparticle Functionality, Technical University of Denmark, 2800 Kgs, Lyngby, Denmark

C. H. Christensen
LORC (Lindoe Offshore Renewables Center), Kystvejen 100, 5330 Munkebo, Denmark
e-mail: chc@lorc.dk

synthesis allows Al to be introduced in the zeolite structure, which allows for tuning the acidic and hydrophobic properties of the zeolite matrix. Furthermore, we present a comprehensive characterization study using BET/N_2-physisorption, inductively coupled ion-plasma optical emission spectroscopy (ICP-OES), powder X-ray diffraction (XRPD), scanning and transmission electron microscopy (SEM and TEM). Our new hybrid material is then compared to the previous synthesized hybrid material in the aerobic oxidation of benzaldehyde and 3,5-dimethylbenzaldehyde see Scheme 1. Hereby, we demonstrate that the presence of embedded Au nanoparticles in the zeolite crystals enhance the selectivity towards the sterically less hindered methylbenzoate for both hybrid materials, thus verifying that the Au metal nanoparticles are truly encapsulated.

To investigate the role of the Au present on the surface of the catalyst, these are removed by a treatment with aqua regia. All four catalysts from the two synthesis strategies, including the Au leaching, are shown in Scheme 2.

The first material termed I-Au@MFI is made as previously described [16] by first immobilizing Au nanoparticles in amorphous silica followed by a hydrothermal synthesis to produce encapsulated Au nanoparticles in crystalline silicalite-1 crystals. During the optional acid leaching the organic template is kept in the micropores of the silicalite-1 crystals, as a filling agent to prevent the aqua regia in dissolving the embedded Au nanoparticles. The effectiveness of this technique, in preventing solvent penetration of the micropore system, has also previously been reported for the constrained desilication of ZSM-5 crystals [17]. The acid leached product is termed II-Au@MFI. In the new 2-step synthesis the first step is to immobilize Au nanoclusters in amorphous silica followed by a hydrothermal synthesis creating silicalite-1 seeds with a higher Au content than the previous product (I-Au@MFI). The resulting silicalite-1 seeds is suspended in a ZSM-5 growth medium containing aluminium and synthesised into the product termed III-Au@MFI. After the optional acid leaching the product is termed IV-Au@MFI.

All the synthesised materials were characterized using XRPD, ICP-OES, N_2 physisorption, SEM and TEM. Furthermore, the catalytic ability of the catalyst materials are tested in the aerobic oxidation of benzaldehyde and 3,5-dimethylbenzaldehyde in methanol to the corresponding methyl esters at room temperature and under atmospheric pressure.

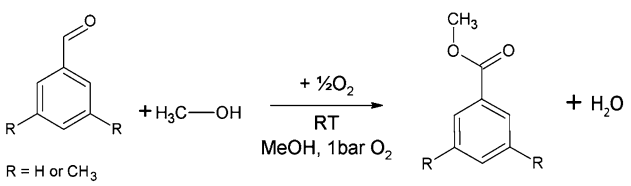

Scheme 1 Reaction scheme for the catalytic test reaction using two different reagent: R = H the stericly unhindered benzaldehyde and R = CH_3 the stericly hindered 3,5-dimethylbenzaldehyde

2 Experimental

2.1 Synthesis and Catalysts Preparation

All chemicals were used as-received without further purification.

2.1.1 Synthesis of I-Au@MFI

The catalyst was prepared as described in our previous study [16].

2.1.2 Synthesis of III-Au@MFI

The gold nanoclusters were prepared as described by Wu et al. [18] equimolarly exchanging the phenylethylthiol for 3-mercaptopropyltrimethoxysilane (MPTMS, Sigma-Aldrich, 95%). 25 mL of the resulting colloidal suspension was diluted with 500 mL THF (Sigma-Aldrich >99%), and 5.25 mL NH_4OH (Merck 25% NH_3) in an Erlenmeyer flask. After stirring (600 rpm) for 15 min 0.39 mL tetraethyl orthosilicate, TEOS (Sigma-Aldrich, 98%) was added and stirred for 8 h. Four additions of TEOS were made at 8 h intervals. The solid precursor product was recovered by evaporation of the solvents at 100 °C overnight. In a beaker 119 g deionized water was mixed with 19 g ethanol, 0.16 g NaOH, and 2.79 g TPAOH (AppliChem, 40 wt%). After obtaining a homogeneous solution 1.23 g precursor was suspended in this and then stirred for 15 min. The suspension was transferred to a 160 mL Teflon lined autoclave, sealed and heated to 100 °C for 5 days. After quenching the autoclave to room temperature the zeolite seeds was recovered by centrifugation at 9,000 rpm for 30 min and decanting off the mother liquid. The solid was washed five times by suspending it in water, centrifuging, and decanting off the mother liquid. Finally, the zeolite seeds were dried at 100 °C overnight. A ZSM-5 growth medium was prepared, by a procedure modified from literature [19], by dissolving 0.079 g NaOH, 0.098 g anhydrous $NaAlO_2$ (Riedel-de Häen, 29.3% Al) in 7.9 mL deionized water under stirring (600 rpm). Silica was added in small portions until 0.876 g SiO_2 gel (SiO_2 gel 100, 0.063–0.2 mm, Merck) had been added. The resulting suspension was mixed by shaking vigorously for 1 h. Then, 0.126 g zeolite seeds were added and shaken another hour. The final catalyst was obtained by sealing the suspension in a 160 mL Teflon lined autoclave and heating it to 180 °C

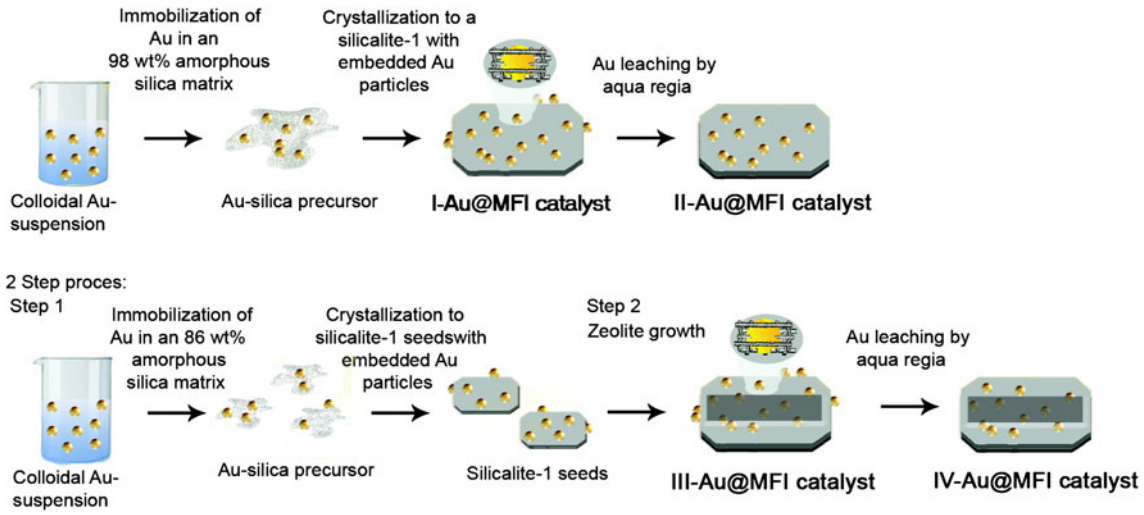

Scheme 2 Synthesis scheme for the four catalysts. The *upper one* is the first strategy and the *lower one* is the 2-step synthesis

for 40 h. After quenching the autoclave to room temperature the zeolite crystals were recovered by filtration on a cellulose filter in a Buchner funnel under suction. Finally, the solid product was washed in deionized water until a pH of 7 was reached. The final product was obtained by drying at 100 °C for 16 h.

2.1.3 Synthesis of II-Au@MFI and IV-Au@MFI

In a typical synthesis 0.4 g un-calcined product of the I-Au@MFI and III-Au@MFI synthesis, respectively, was transferred to a sintered glass frit filter (#4) and washed in 5 mL deionized water under suction. The solid was then washed in 25 mL aqua regia in portions of four each separated by washing in 5 mL deionized water. Finally, the acid was removed by washing in 200 mL deionized water.

2.1.4 Calcination

All four prepared Au@MFI samples are ground in a mortar and calcined in air by heating in a muffle oven. The samples are heated in a ceramic crucible to 550 °C at a ramp of 2 °C/min. The samples are held at this temperature for 3 h to ensure complete decomposition of the organic templates, after which it is allowed to cool naturally to room temperature.

2.2 Characterizations Methods

To identify and verify the crystal structure of the products, XRPD patterns were recorded using a Philips PANalytical X'PERT powder diffractometer with Cu Kα radiation in the 2θ interval 5–70°. The elemental analysis were preformed by ICP-OES and used to determine the exact amount of Au in the Au@MFI samples.

The surface area and the pore volume were determined by nitrogen adsorption and desorption measurements at liquid nitrogen temperature on a Micromeritics ASAP 2020. The samples were outgassed in vacuum at 473 K for 6 h prior to measurements. The total surface area was calculated according to the BET method and the micropore volumes were determined by the *t*-plot method [20].

The crystal size, morphology of the zeolite, and amount of highly reflecting Au of the Au@MFI samples were examined by scanning electron microscopy (SEM) on a Phillips XL20 FEG using a backscatter detector. The samples were placed on a carbon film and 20 nm Pt/Pd was evaporated onto the sample to achieve sufficient conductivity.

To investigate the size of the Au particles and the effect of the acid leaching sample I-Au@MFI and II-Au@MFI were examined by transmission electron microscopy (TEM) on a Titan 80–300 SuperTwin electronmicroscope operated at 300 kV. The samples were measured after calcination and then placed on a Cu-grid with a lacey carbon film.

2.3 Catalytic Aerobic Oxidation of Aldehydes

All reagents used were of reagent grade and used without further purification: Benzaldehyde (C_7H_6O, 99%, Sigma-Aldrich), 3,5-dimethylbenzaldehyde ($C_9H_{10}O$, 97%, Sigma-Aldrich), methanol (CH_3OH, 99%, Sigma-Aldrich), 30 wt% sodium methoxide solution (Sigma-Aldrich), anisol (C_7H_8O, 99% Sigma-Aldrich).

In a typical experiment, a mixture of 0.5 mmol aldehyde (benzaldehyde or 3,5-dimethylbenzaldehyde), 60 mmol methanol and 0.1 mmol sodium methoxide were charged into a 10 mL two-neck round-bottom flask equipped with a

condenser and a septum together with a Au@MFI catalyst (0.1 mol% Au). The reactor system was connected to an O_2 cylinder and flushed with O_2. The reaction mixture was mixed with magnetic stirring and small samples were taken at selected times, filtered directly through a syringe filter and analysed by GC and GC–MS. The GC column Agilent Technologies Inc. HP-5 was used. The amounts of substrates and products were quantified using anisol as internal standard.

3 Results and Discussion

3.1 Characterization of the Au Zeolite Hybrid Materials

The XRPD patterns for the four Au@MFI catalysts are all shown in Fig. 1. All patterns are recorded after the zeolite synthesis and prior to combustion of the organic template. From Fig. 1 it is clearly seen that all samples contain highly crystalline material with the MFI structure [21] along with Au particles [22].

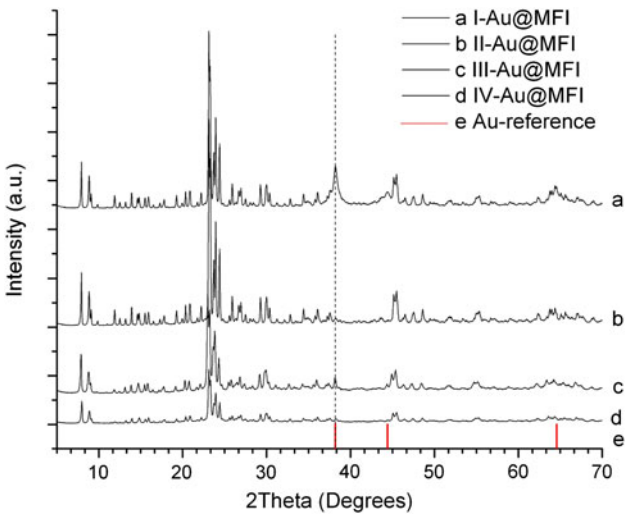

Fig. 1 XRPD patterns of **a** I-Au@MFI, **b** II-Au@MFI, **c** III-Au@MFI and **d** IV-Au@MFI. A reference pattern [22] **e** for bulk Au is shown as *bars* below the experimental patterns. All patterns are recorded before combustion of the organic template

The average diameter of the Au particles in the [111] crystal direction is estimated by the Debye–Scherrer equation and listed in Table 1. In Table 1 is also given the Au content determined from elementary analysis, ICP-OES, and the results from N_2 physisorption measurements are also given.

Comparing the average Au particle size before and after calcination yields the same trend for both sets of preparation methods. The overall trend is that the Au [111] sizes increase significantly for all samples. However, the most significant increase is for the two parent samples: I-Au@MFI (a factor of $\sim$5.1) and III-Au@MFI (a factor of >1.6). It is assumed that this is due to the larger amount of Au particles on the surface of the parent samples, which may sinter freely, compared to the two washed samples, II-Au@MFI (a factor of $\sim$1.5) and IV-Au@MFI (a factor of $\sim$1.3). However, it could not be ruled out that the effect originates from the lower gold loading of the leached samples, i.e., nanoparticle dispersion. It is anticipated that the acid leaching decreases the average Au particle size since all the small Au particles should primarily be embedded in the zeolite and therefore inaccessible to the acid. This appears to be invalid in going from sample I-Au@MFI to II-Au@MFI. Here, the average diameter has increased from 18 to 28 nm prior to calcination. This could be due to the presence of small gold particles on the surface that would be removed first during the acid leaching leaving behind the larger Au particles resulting in an increase in the relative amount of larger particles. Opposed to this sample III-Au@MFI shows a small but net decrease in average diameter in going from sample III-Au@MFI to sample IV-Au@MFI. The Au content determined from ICP-OES analysis show that a significant amount of Au is lost during the acid leaching. However, the amounts of Au lost from the two acid leached samples are comparable, i.e., ca. 20%. Comparing the two parent samples, I-Au@MFI and III-Au@MFI, there is a considerable difference in the amount of Au demonstrating that the second synthesis routes gives a product containing an increased amount of Au.

Table 1 The average Au particle size before and after calcinations, Au content measured by ICP-OES and N_2 physisorption data. Au content and N_2 physisorption measurements are recorded after the combustion of the organic template

Material	Au size before/after calcination (nm)[a]	Au content (wt%)	Surface area (m^2/g)[b]	Micropore volume (cm^3/g)[c]	Zeolite size (μm)[d]
I-Au@MFI	18/92	1.37	306 [16]	0.096 [16]	2
II-Au@MFI	28/41	0.25	329	0.112	2
III-Au@MFI	64/ >100	3.34	245	0.105	10
IV-Au@MFI	49/63	0.65	269	0.093	10

[a] Estimated by Scherrer Equation D[111][b]Calculated by BET[c]Calculated by *t*-plot method[d]Estimated from SEM

This is believed to be due to a loss of either Au (I-Au@MFI) or zeolite precursor (III-Au@MFI) during the synthesis or a combination; this could not be verified from the available data.

In Table 1 the BET surface areas and micropore volumes of the four Au@MFI sample are given. The surface area for I-Au@MFI and II-Au@MFI lie in the range of previous results for conventional MFI samples around 300 m^2/g [23, 24]. The surface areas for III-Au@MFI and IV-Au@MFI are lower than for the former, which the authors speculate might be due to either crystal size, micropore blockage by the incorporated Au nanoparticles or extra framework alumina, or a very small amount of amorphous material. The latter, however, seems contradicted as the XRPD pattern shows only crystalline zeolite and gold. The micropore volumes for all four Au@MFI lie in the range of previous results [23, 24]. The surface area and micropore volume for the four Au@MFI samples illustrate that in spite of the incorporation of gold particles in the materials they are expected to perform like a conventional zeolite in respect to size-selectivity.

The SEM images of the four Au@MFI samples are shown in Fig. 2 and the images are recorded using the backscatter detector. By using the backscatter detector the Au particles, which are highly reflecting particles, will appear as bright spots.

Comparing sample I-Au@MFI and II-Au@MFI (Fig. 2a, b) there is a clear reduction in the amount of Au particles on the MFI crystal surfaces after the acid leaching in Fig. 2b. Note that only two larger Au particles are still observed after the treatment and that all smaller particles have disappeared from view. This observation indicates that the dissolution strategy has worked as intended. It should be emphasized that the resolution of the SEM images does not allow for detection of the small Au particles dominating this sample and the conclusions are only based on the larger particle agglomerates. From the SEM images of sample I-Au@MFI and II-Au@MFI it can be observed that a homogeneous distribution exists concerning the size of the MFI crystals of around 2 μm (Fig. 2a, b). From the SEM images it can also be seen that the crystals are primarily the typical coffin-shaped morphology for MFI-zeolites [23, 24]. Some twinned and some highly inter-grown crystals are also observed for the two samples. The acid treatment has not had a detectable influence on the morphology of the zeolites. Figure 2c, d show the 2-step synthesis strategy before and after acid leaching (sample III-Au@MFI and IV-Au@MFI). Comparing the two images one can observe a smaller amount of the high reflecting Au particle agglomerates on the crystal surface of the acid leached sample. The size and morphology of the zeolite does not change during the acid leaching. The MFI crystals are significantly larger for the 2-step synthesis compared to the first. The crystals are around 10 μm and have less distinct and less smooth morphologies than the previous, although the overall morphology is still coffin

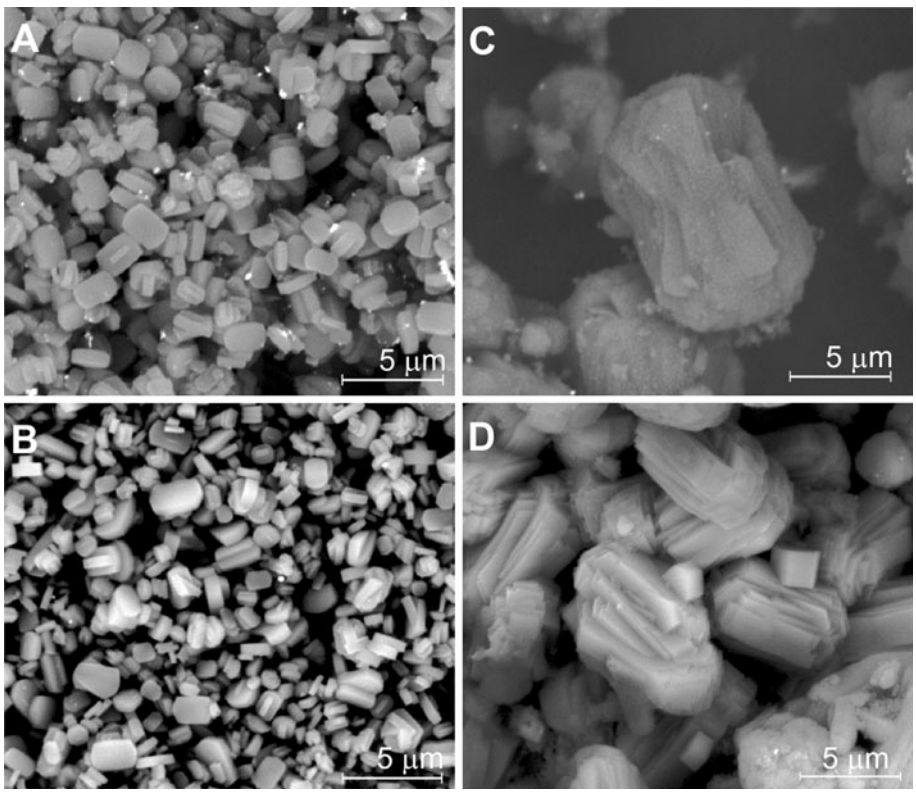

Fig. 2 SEM images of **a** I-Au@MFI, **b** II-Au@MFI, **c** III-Au@MFI, and **d** IV-Au@MFI. The images are recorded using the backscatter detector and after combustion of the template

shaped-like. The differences in size and morphology are ascribed to the difference in synthesis procedures. The ratio of silica to aluminium in the zeolite is estimated by EDS measurement to be 14 prior to acid treatment and 21 after. This shows that the 2-step synthesis results in a zeolite which may be made acidic by ion-exchange making it a potentially bi-functional catalyst and that the acid treatment dealuminates the sample slightly. In summary the silicalite-1 zeolites (I- and II-Au@MFI) are apparently unaffected by the aqua regia in terms of both morphology and crystallinity as seen from SEM and XRPD, respectively. The Al-containing zeolites (III- and IV-Au@MFI) lose a significant amount of Al, the morphology remains unchanged, and the crystallinity is only slightly decreased by the aqua regia treatment. As the catalytic activity of Au is governed by the presence of catalytic amounts of base [25], it is not relevant to test an acid form of the catalysts, as reaction with the base would result in the Na-form and a loss of activity. The Al-containing catalysts (III- and IV-Au@MFI) still contain some Lewis acidity in the tested Na-form; however, this is not expected to affect the activity.

To investigate the size of the Au particles, and whether the Au particles are on the external surface of the MFI crystals after the acid leaching, TEM is used. The larger MFI crystals of samples III- and IV-Au@MFI make a TEM investigation impossible thus only the TEM investigation of I- and II-Au@MFI are shown here. In Fig. 3 representative TEM images of samples I- and II-Au@MFI are shown. In these images the gold particles are seen as dark particles both in profile view, i.e., on the edge of the zeolite crystal perimeter and in the plane view, i.e., on the centre of the zeolite crystals.

In Fig. 3a the smaller particles (1–3 nm) are concentrated in the centre of the plane view but are also present in the profile view together with larger agglomerated particles (>20 nm). These particles are all much larger than the cages present in the MFI zeolite, indicating that the framework have been disrupted to accommodate the Au particles. It is well known that only small Au particles are active in catalysis [1, 26, 27]. Therefore, the small particles on the outer surface of the zeolite will result in unselective catalytic activity. These particles are thus the most important to remove by the acid treatment. A representative TEM image of the acid leached sample II-Au@MFI is shown in Fig. 3b. It is seen that all the particles, in the profile view, have been removed leaving the small particles in the plane view intact. Throughout the sample all the small Au particles on the external surface appears to be removed while few large particles remain. From this it is concluded that if all the small particles had been accessible to the acid treatment no small particles would be left. We have previously determined by TEM tomography that most

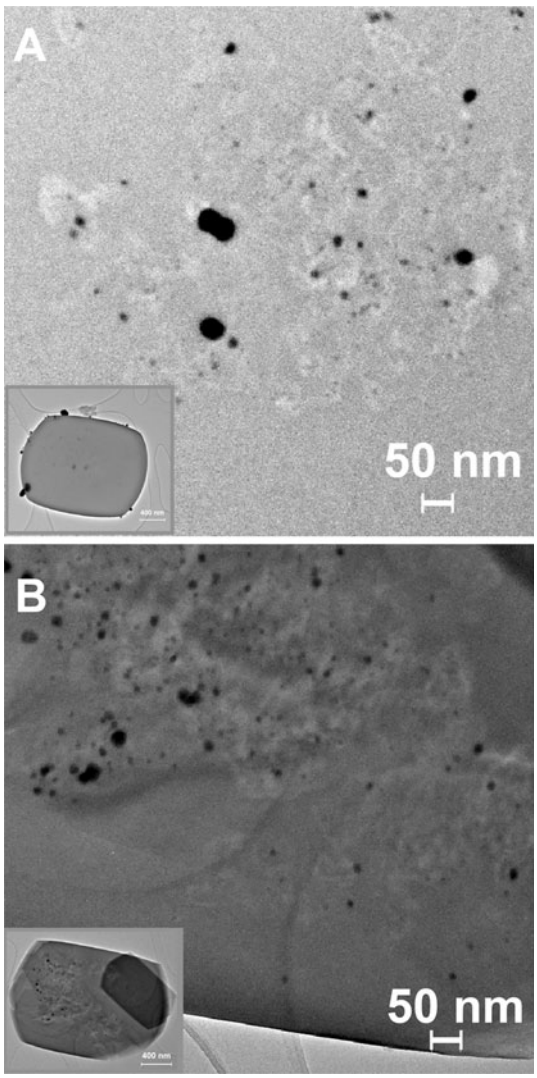

Fig. 3 A magnified TEM image of **a** I-Au@MFI and **b** II-Au@MFI. The *scale bars* in the images are 50 nm and in the *inset* they are 400 nm

of the Au particles in the plane view of sample I-Au@MFI are embedded in the MFI crystal [16]. Hence, it seems likely that the small Au particles left by the acid treatment are also the ones incorporated into the zeolite. The strategy of removing the small particles on the outer surface by leaving the template molecule in the pores while washing with aqua regia has been effective. It is worth noting that from the presented data the selectivity of the acid treatment has only been qualitatively demonstrated and is not expected to be completely selective. The novel discovery of this work is, however, that the acid treatment is selective and this opens the possibility to remove all Au from the surfaces leaving only the catalytic active particles. These results are consistent with the assumptions made previously in the XRPD investigation, i.e., that the average Au diameter increases on acid leaching due to the faster dissolution of the small Au particles on the external surface.

Furthermore in the TEM images small areas of lower contrast are observed surrounding the Au particles. This is attributed to areas of mesoporosity arising when the Au nanoparticles are incorporated in the framework accompanied by disruption of the crystal structure. Note that this porosity does not show in the physisorption and hence it must be of insignificant concentration.

3.2 Catalytic Experiments

It is well known that Au nanoparticles can oxidise aldehydes to esters [25, 28]. The four Au@MFI catalysts are tested in the size-selective oxidation of benzaldehyde and 3,5-dimethylbenzaldehyde, see Scheme 3.

The benzaldehyde molecules should be able to diffuse into the zeolite crystals and be oxidized by the embedded gold particles. Whereas, the more bulky 3,5-dimethylbenzaldehyde molecules can only be oxidized by gold nanoparticles located on the outside of the zeolite crystals. The activity measurements are illustrated in Fig. 4 as yield of methyl esters as a function of time.

In Fig. 4a the catalytic activity for I-Au@MFI and II-Au@MFI in the oxidation of both benzaldehyde and 3,5-dimethylbenzaldehyde is shown. It is seen that both I-Au@MFI and II-Au@MFI are able to catalyse the oxidation of benzaldehyde giving yield of 97 and 94%, respectively, after 72 h at full conversion (>99%). The major by-product is benzoic acid in <6% yield, as previously observed in literature [28]. In the case of 3,5-dimethylbenzaldehyde the activities are much lower for the two catalysts resulting in yields of <3% with conversion <5% after 72 h. In Fig. 4b the catalytic activities of III-Au@MFI and IV-Au@MFI are shown. It shows that III-Au@MFI and VI-Au@MFI have the same selectivity in the oxidation of benzaldehyde and 3,5-dimethylbenzaldehyde as I-Au@MFI and II-Au@MFI. However, the yields and conversions are a little lower for the methyl benzoate but comparable for the methyl 3,5-dimethylbenzoate.

The catalytic result proves that the embedded gold nanoparticles are accessible and catalytic active through zeolite micropores since it is possible to oxidise benzaldehyde. Furthermore, as it is not possible to oxidise the more bulky 3,5-dimethylbenzaldehyde, it is only the

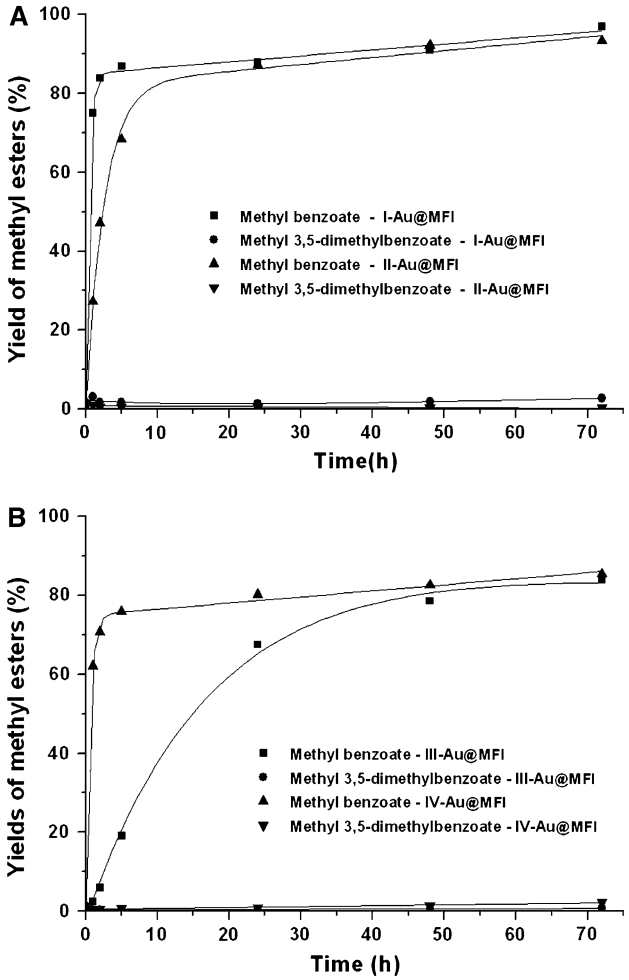

Fig. 4 Yields as a function of time for **a** I-Au@MFI and II-Au@MFI and **b** III-Au@MFI and IV-Au@MFI. The catalytic tests were carried out in an open flask at room temperature, atmospheric pressure and with the following ratios: Aldehyde: 5; CH_3OH: 600; $NaOCH_3$: 1 and with 0.1 mol% Au@MFI

embedded gold particles, which are catalytically active. Regarding the washing of the catalysts with aqua regia, it was expected that the catalytic activity in the oxidation of 3,5-dimethylbenzaldehyde would decrease when removing the Au particles on the surface. However, at these conversions no clear change in the catalytic activities was observed. As a reference catalyst Au on TiO_2 (Mintek,

Scheme 3 Schematic drawing of the size-selectivity in the benzaldehyde and 3,5-dimethylbenzaldehyde oxidation reaction

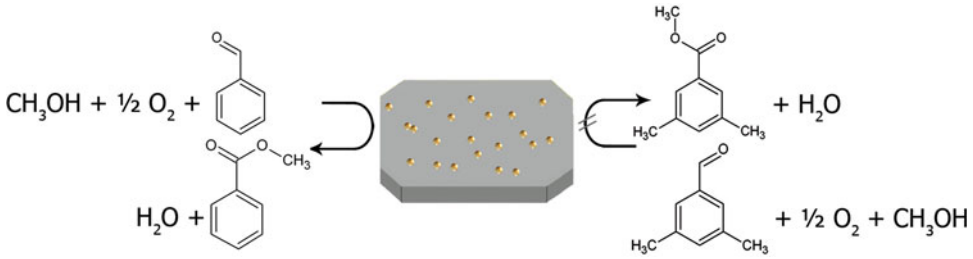

1 wt%) was tested. It showed no shape-selectivity and was highly cable of oxidising both benzaldehyde and 3,5-dimethylbenzaldehyde. The small difference in activity and selectivity for the catalysts before and after acid leaching can be ascribed to sintering of the small Au nanoparticles on the external surface of the zeolite crystals during calcinations. Meaning that after calcination very few active particles remain on the surface of the parent samples. The effect of the average Au nanoparticles size determined from XRPD (Table 1) could not be correlated to the catalyst activity. The authors speculate that this is due to the broad particle distribution, which makes it impossible to determine the amount or average size of the active Au nanoparticles, i.e., with a diameter of less than 10 nm [1, 26, 27]. The catalytic results also show that the Au nanoparticles are active even after calcinations at 550 °C hereby verifying that the Au nanoparticles are sinter-stable when encapsulated.

4 Conclusions

In conclusion we have studied the catalytic activities of hybrid materials comprising sinter-stable Au nanoparticles accessible only through zeolite micropores. We have shown two different synthesis strategies to prepare MFI type zeolite crystals, which contain embedded Au nanoparticles in the range of 1-3 nm. Aluminium was successfully introduced in the zeolite matrix yielding opportunities to tune the material properties. Furthermore, the effect of post aqua regia treatment to remove Au agglomerates on the external surface of the MFI type zeolite has been studied. By TEM it was shown that all the small Au nanoparticles on the external surface of the hybrid material were removed by acid leaching. No significant change in activity for catalysts III- and IV-Au@MFI, which have some Lewis acid sites due to the presence of Al, was observed. This is in line with the expectations as the aerobic oxidations using gold rely on a catalytic amount of base. Future work will include the utilization of the bi-functionality of catalysts III- and IV-Au@MFI, for a reaction requiring both acidic and oxidative properties.

Moreover, the hybrid materials were tested in the aerobic oxidation of benzaldehyde and 3,5-dimethylbenzaldehyde in methanol to the corresponding methyl esters. The reactions were conducted at room temperature and under atmospheric pressure. The materials were active as substrate-size selective oxidation catalysts for in the aerobic oxidations. We have shown that it is not possible to oxidize 3,5-dimethylbenzaldehyde whereas benzaldehyde is readily oxidized to the methylester very selectively, thus showing that the encapsulated Au nanoparticles are only accessible through the zeolite micropores.

Acknowledgments The Centre for Catalysis and Sustainable Chemistry is sponsored by the Danish National Research Foundation. We gratefully acknowledge the assistance of Eva Charlotte Bendixen and Aino Nielsen at Haldor Topsøe A/S for obtaining the TEM and SEM images, respectively.

References

1. Haruta M (2003) Chem Rec 3:75
2. Haruta M, Yamada N, Kobayashi T, Iilima S (1997) J Catal 115:301
3. Valden M, Lai X, Goodman DW (1998) Science 281:1674
4. Bartholomew CH (1997) Stud Surf Sci Catal 111:585
5. Haruta M (1997) Catal Today 36:153
6. Arnal PM, Comotti M, Schüth F (2006) Angew Chem Int Ed 45:8224
7. Ren N, Yang Y-H, Shen J, Zhang Y-H, Xu H-L, Gao Z, Tang Y (2007) J Catal 251:182
8. Joo SH, Park JY, Tsung C-K, Yamada Y, Yang P (2009) Nature Mater 8:126
9. Beakley LW, Yost SE, Cheng R, Chandler BD (2005) Appl Catal A 292:124
10. Corma A (1995) Chem Rev 95:559
11. Corma A (1997) Chem Rev 97:2373
12. Fierro-Gonzalez JC, Hao Y, Gates BC (2007) J Phys Chem C 111:6645
13. Kuge K, Calzaferri G (2003) Microporous Mesoporous Mater 66:15
14. Guillemot D, Polisset-Thfoin M, Fraissard J (1996) Catal Lett 41:143
15. Liu X, Dilger H, Eichel RA, Kunstmann J, Roduner E (2006) J Phys Chem B 110:2013
16. Laursen AB, Højholt KT, Simonsen SB, Lundegaard LF, Helveg S, Schüth F, Paul M, Grunwaldt J-D, Kegnæs S, Christensen CH, Egeblad K (2010) Angew Chem Int Ed 49:3504
17. Pérez-Ramírez J, Abelló S, Bonilla A, Groen JC (2009) Adv Funct Mater 19:164
18. Wu Z, Suhan J, Jin R (2009) J Mater Chem 19:622
19. Lechert H, Kleinwort R (2001) High-Alumina ZSM-5. In: Robson H, Lillerud KP (eds) Verified syntheses of zeolitic materials, 2nd revised edn. Elsevier Science BV, Amsterdam. http://www.iza-online.org/synthesis/Recipes/High-Alumina%20ZSM-5.html
20. Lippens JH, de Boer J (1965) J Catal 4:319
21. Baerlocher CH, McCusker LB (2007) IZA database of zeolite structures. http://www.iza-structure.org/databases/
22. Hanawalt et al. (1938) Anal Chem 10: 475 (ICSD XRPD pattern for Au, reference PDF# 00-001-1172)
23. Kustova MY, Rasmussen SB, Kustov AL, Christensen CH (2006) Appl Catal B 67:60
24. Egeblad K, Kustova M, Klitgaard SK, Zhu K, Christensen CH (2007) Microporous Mesoporous Mater 101:214
25. Marsden C, Taarning E, Hansen D, Johansen L, Klitgaard SK, Egeblad K, Christensen CH (2008) Green Chem 10:168
26. Wolf A, Schüth F (2002) Appl Catal A 226:1
27. Haider P, Kimmerle B, Krumeich F, Kleist W, Grunwaldt J-D, Baiker A (2008) Catal Lett 125:169
28. Klitgaard SK, DeLaRiva AT, Helveg S, Werchmeister RM, Christensen CH (2008) Catal Lett 126:213